Plasmonics of regular shape particles, a simple group theory approach

Sarra Mitiche, Sylvie Marguet, Fabrice Charra, Ludovic Douillard

Plasmonics of Regulary Shaped Particles, A Simple Group Theory Approach

Sarra Mitiche[1], Sylvie Marguet[2], Fabrice Charra[1] and Ludovic Douillard.[1]*

[1]SPEC CNRS CEA Université Paris-Saclay, France
[2]NIMBE CNRS CEA Université Paris-Saclay, France

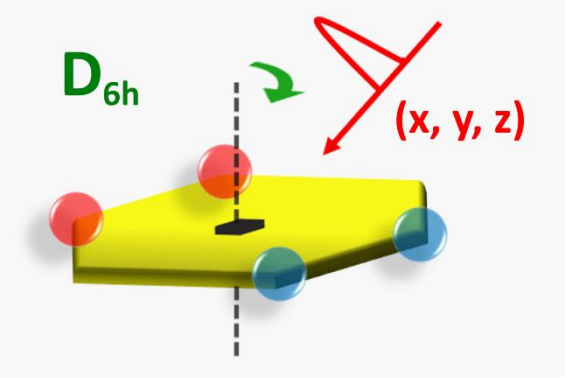

A simple group theory method to describe the plasmonic response of particle of finite or infinite symmetry point groups.

Provide the authors' website if possible.

Sylvie Marguet http://iramis.cea.fr/Pisp/sylvie.marguet/

Fabrice Charra http://iramis.cea.fr/en/Pisp/fabrice.charra/

Ludovic Douillard http://iramis.cea.fr/Pisp/ludovic.douillard/

Nano Research

ISSN 1998-0124 CN 11-5974/O4
https://doi.org/(automatically inserted by the publisher)

Plasmonics of Regulary Shaped Particles, A Simple Group Theory Approach

Sarra Mitiche[1†], Sylvie Marguet[2], Fabrice Charra[1] and Ludovic Douillard[1](✉)

[1]*SPEC CNRS CEA, Université Paris-Saclay, Gif sur Yvette F-91191, France*
[2]*NIMBE CNRS CEA, Université Paris-Saclay, Gif sur Yvette F-91191, France*
[†]*PPSM CNRS ENS Paris-Saclay, Université Paris-Saclay, Cachan F-94230, France*

Received: day month year / **Revised:** day month year / **Accepted:** day month year (automatically inserted by the publisher)

ABSTRACT

A simple hand calculation method based on group theory is proposed to predict the near field maps of finite metallic nanoparticles of canonical geometries: prism, cube, hexagon, disk, sphere, etc corresponding to low order localized surface plasmon resonance excitations. In this article, we report the principles of the group theory approach and demonstrate, through several examples, the general character of the group theory method which can be applied to describe the plasmonic response of particle of finite or infinite symmetry point groups. Experimental validation is achieved by collection of high-resolution subwavelength near-field maps by photoemission electron microscopy (PEEM) on a representative set of Au colloidal particles exhibiting either finite (hexagon) or infinite (disk, sphere) symmetry point groups.

KEYWORDS

Surface plasmon resonance, group theory, hexagon, disk, sphere, photoemission electron microscopy (PEEM).

1. Introduction

Surface plasmons [1] provide a unique opportunity for the light manipulation at the nanometer scale. In the case of a metallic nanoparticle (MNP), the excitation of a plasmon resonance generates intense electromagnetic fields located at specific points on its surface, called **hot spots**. At these points, light is confined in subwavelength distances (< 20 nm) and field amplitudes are large [2, 3]. The ability to produce and control hot spots offers great promises for many applications, including sensing [4–6], heating [7, 8], photosynthesis [9,10], oncology [11–13], imaging [14, 15], computer science [16] and many others. In view of the technological applications envisaged, it is necessary to develop simple methods to investigate this phenomenon.

The positions of hot spots in a nanoparticle depend on both its geometry and the configuration of the exciting electromagnetic wave. The distribution of hot spots in any nano-object can be quantitatively determined by numerical simulations using advanced methods such as the Finite Difference Time Domain (FDTD) [17–19] or the Discrete Dipole Approximation (DDA) [20, 21]. However, these methods require large computational memory and long calculation times. In this work, we propose a simple and fast analytic method to predict the hot spot spatial distributions of a basic shape nanostructure by a simple hand calculation. In short, the hot spot positions are extracted from the particle and electromagnetic wave symmetries using group theory.

The group theory is a mathematical approach used in chemistry to predict and to analyze the physicochemical properties of matter based on its symmetry. One important representative example is the use of the group theory to build the orbitals of a molecule. A fundamental step of this approach is the determination of an orthonormal set of functions acting as basis vectors for the irreducible representations of the molecule symmetry point group. These functions, commonly called **symmetry adapted linear combinations (SALC)**, are usually linear combinations of the atomic orbitals of the molecule [22–24]. In the proposed method, an equivalent approach is adopted to predict and to interpret the plasmonic behaviour of a metallic nanoparticle. The distribution of the hot spots due to the excitation of a plasmon mode is deduced from the particle symmetry and that of the exciting electric field. Indeed, the determination of the SALC eigenstates of a nanoparticle under excitation gives a direct image of its plasmon charge distribution which corresponds to the hot spot positions.

In our previous works, we successfully applied the group theory approach to determine the plasmonic responses of 2D-(triangle [25]) and 3D-(cube [26]) metallic nanoparticles, all objects of finite numbers of symmetry elements. However, difficulties arise when a particle possesses an infinite number of symmetry elements as encountered in the cases of a rod, a disk, a sphere, etc. In this article, we extend and generalize the proposed approach to the case of particles of infinite symmetry.

The first part of the article is a concise description of the group theory method as applied to the case of objects of finite symmetry. As an example, the plasmonic response of a thin hexagonal particle is described. In the second part, we expose the method generalization so as to determine the plasmonic response of objects

Address correspondence to Ludovic Douillard. ludovic.douillard@cea.fr.

of infinite symmetry. In this regard, two canonical particle shapes are considered, namely disk (2D-MNP) and spherical (3D-MNP) shapes. Experimental validations are carried out by mapping the near field distributions using the photoemission electron microscopy (PEEM) [27, 28].

2. Experimental

2.1. Sample preparation

Single-crystalline Au nanoparticles (spheres, hexagons, disks) were prepared following already published protocols, based on the seed mediated growth [26, 29–31]. The chemical reduction of hydrogen tetrachloroaurate (III) hydrate ($HAuCl_{14}$:$3H_2O$) was carried out in aqueous solution in the presence of cetyltrimethylammonium bromide (CTAB) as the capping agent. Ultra-smooth and highly uniform spheres were obtained following the multistep procedure reported by Wang's group [30]. Spheres of increasing sizes were produced through overgrowth of smaller ones, followed by an oxidation step of the intermediate polyhedrons [30]. Here, spherical 40-nm nanoparticles resulting from mild oxidation of 60-nm cubes were employed as seeds in the first step of the growth [26]. Three successive steps of growth and mild oxidation were required to produce highly spherical spheres with an average diameter of 98 ± 1nm. The oxidant complex Au(III)/CTAB was used to reshape intermediate nanocrystals into rounded shapes by smoothing the vertices and edges, as explained elsewhere [29, 30]. To grow 150-200 nm (in-plane height) hexagons, a method initially proposed by Mirkin's group to produce triangular nanoplates was adapted [31]. By optimizing the concentrations of the reactants in the growth solution, i.e. CTAB 0.1 M, $HAuCl_{14}$0.7 mM and ascorbic acid 1.6 mM, a high percentage of hexagonal nanoplates (~90%) was obtained to the detriment of triangular shapes (~10%). These nanoplates were purified through selective sedimentation to the bottom of the tube while the polyhedral byproducts (~50%) remained in the supernatant. Nanodisks 92 nm in diameter were obtained by mild oxidation of slightly larger hexagonal nanoplates using the same oxidizing complex as for the spheres. The PEEM samples were prepared by depositing a drop of the corresponding nanoparticles solution on an ITO/SiO_2 substrate (PGO CEC0505S, ≤ 50 Ω/sq) and then cleaned by UV/Ozone [32] to remove any organic residues.

2.2. PEEM Imaging

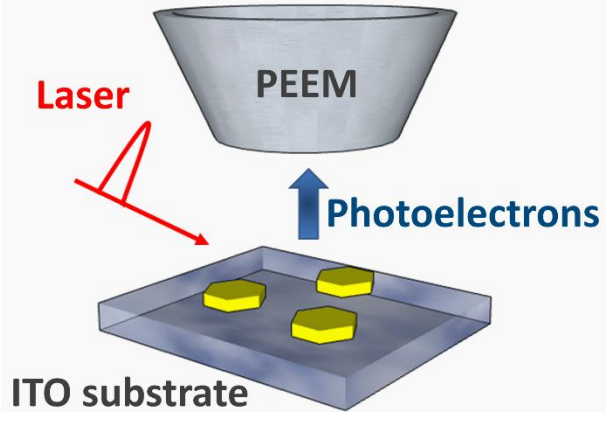

Figure 1 Schematic representation of the PEEM experimental setup

Plasmon field maps are acquired with photoemission electron microscopy (PEEM), whose working principle is recalled in Fig.1 [33–38]. A nonlinear multiphotonic photoemission process is strongly enhanced upon excitation of surface plasmons. The collected photoelectrons associated with a localised surface plasmon resonance reflect the actual spatial plasmon field distribution at the surface of the metallic nanostructure under investigation. The photoemission electron microscope used is a commercial Elmitec SPELEEM III operating in ultra-high vacuum at pressure in the low range of 10^{-10} mbar. The routine spatial resolution is about 20 nm.

In this setup, the nano-objects are excited at grazing incidence (angle α = 72.5 ± 2° between laser beam k-vector and surface normal), in the visible wavelength range (520-640 nm: 2.38-1.94 eV), with the pulsed output of an optical parametric oscillator (Chameleon OPO, Coherent Inc.) pumped by a mode-locked Ti:sapphire oscillator (Chameleon Ultra II, Coherent Inc., repetition rate 80 MHz, pulse width 140 fs) and, in the infrared wavelength range IR (710-1050 nm; 1.75-1.18 eV), directly with the pulsed output of the mode-locked Ti:sapphire oscillator. The peak power densities at the sample surface are tuned from 50 to 500 MW/cm². The polarization of the laser beam is adjusted from *P* to *S* polarization with the help of a half-wave plate allowing a selective excitation of plasmon modes.

In addition to the near optical field maps, images of the particle topography, with a spatial resolution close to 10 nm, can be obtained using backscattered electrons in the low-energy electron microscopy (LEEM) imaging mode [39]. Both PEEM and LEEM images can be combined in order to correlate the near optical field distribution to the particle topography.

3. Results and Discussion

3.1. Particles of finite symmetry

The first step of the group theory method is to define the point group symmetry [23] of the considered particle. A flat particle of hexagonal symmetry possesses a D_{6h} symmetry (not considering any substrate). In more details, a hexagon is invariant following a rotation of a 2π/6 angle around an axis perpendicular to its plane (C_6 rotation axis along the z axis). It presents also six C_2 in-plane rotation axes, six vertical symmetry planes σ_{dv}, an horizontal symmetry plane σ_h and a centre of inversion *i* (see Fig. S1 in the Electronic Supplementary Material (ESM)). So, a regular hexagonal particle possesses a finite number of symmetry elements. The corresponding character table is given in Table 1.

In a second step, we determine the **irreducible representation (irrep)** [22, 23] Γ_{ext} of the external electric field $\overrightarrow{E_{ext}}$. The latter is deduced from the exciting wave symmetry and the character table of the considered particle. In the case of a regular hexagonal particle excited with an electromagnetic wave polarized linearly, $\overrightarrow{E_{ext}}$ is vectorial in nature $\overrightarrow{E_{ext}}$ = ($E_{ext,x}$, $E_{ext,y}$, $E_{ext,z}$) and transforms like the translation vectors (x, y, z). So, according to the character table of the D_{6h} point group, the in-plane (x, y) component transforms like the irrep E_{1u} and the normal z component transforms like the irrep A_{2u} (see Table 1). In the following, the z component of $\overrightarrow{E_{ext}}$ will not be further considered since the particle under investigation is essentially an xy-two-dimensional structure. Indeed, plasmon resonances normal to the particle plane are expected in the deep blue wavelength range, where absorption losses of most noble metals forbid any coherent plasmon oscillation. So, only in-plane surface plasmon resonances are further on considered.

	E	$2C_6$	$2C_3$	C_2	$3C'_2$	$3C''_2$	i	$2S_3$	$2S_6$	σ_h	$3\sigma_d$	$3\sigma_v$	Linear, rotations
A_{1g}	1	1	1	1	1	1	1	1	1	1	1	1	
A_{2g}	1	1	1	1	-1	-1	1	1	1	1	-1	-1	R_z
B_{1g}	1	-1	1	-1	1	-1	1	-1	1	-1	1	-1	
B_{2g}	1	-1	1	-1	-1	1	1	-1	1	-1	-1	1	
E_{1g}	2	1	-1	-2	0	0	2	1	-1	-2	0	0	(R_x, R_y)
E_{2g}	2	-1	-1	2	0	0	2	-1	-1	2	0	0	
A_{1u}	1	1	1	1	1	1	-1	-1	-1	-1	-1	-1	
A_{2u}	1	1	1	1	-1	-1	-1	-1	-1	-1	1	1	z
B_{1u}	1	-1	1	-1	1	-1	-1	1	-1	1	-1	1	
B_{2u}	1	-1	1	-1	-1	1	-1	1	-1	1	1	-1	
E_{1u}	2	1	-1	-2	0	0	-2	-1	1	2	0	0	(x, y)
E_{2u}	2	-1	-1	2	0	0	-2	1	1	-2	0	0	

Table 1 Character table for D_{6h} point group [40]. Following standard conventions, the principal order rotation axis (C_6) is taken as the z axis of the Cartesian reference coordinate system (Ox, Oy, Oz). Red lines represent the irreducible representations of the $\overrightarrow{E_{ext}}$ components.

Plasmon modes that can be excited with an external electric field $\overrightarrow{E_{ext}}$ are called **optically active** (bright modes). For a plasmon mode of a given symmetry particle to be excited by an external electric field, its irrep and that of the exciting field have to fulfil a vectorial selection rule as demonstrated by *Zhang et al*. [41]. More precisely, this vectorial selection rule states that if the i^{th} component i = (x, y, z) of the electric field $\overrightarrow{E_n}$ of a plasmon mode indexed n transforms as the irrep $\Gamma_{n,i}$, respectively that of an external field $\overrightarrow{E_{ext}}$ transforms as the irrep $\Gamma_{ext,i}$, then the excitation strength of the resonance mode n $\langle E_n | E_{ext} \rangle$ vanishes unless there is a product $\Gamma_{n,I} \otimes \Gamma_{ext,i}$ transforming as the **totally symmetric irrep A**. So, for a hexagonal MNP illuminated with an electromagnetic wave polarized linearly, only the 2-dimensional irrep E_{1u} contains modes with non-zero electric dipole moment in the xy plane (bright modes). The details of the calculation are given in ESM.

Based on the above symmetry considerations, the final step consists in determining the **charge distribution of the plasmon mode under investigation**. A localised surface plasmon resonance corresponds to an accumulation of surface charges at specific angular points of the object: corners, edges, or faces [34, 42–47]. Either positive or negative, these induced charges can be described by virtual s-atomic orbitals attached to specific sites at the object surface. A hexagonal particle presents geometry singularities (corners) at the positions of which electrical charges can accumulate, so one natural choice for the definition of the default basis vectors is to attach s-atomic orbitals to the six object vertices. The plasmonic charge distribution corresponds to the determination of the SALC eigenstates. This operation is conducted by application of the projector operator (Van Vleck operator – see ESM) associated to the irrep of the considered plasmon mode to the basis function set. In practice, a first eigenstate is determined by projection of any of the basis vector. For a hexagonal particle, one charge distribution eigenstate of E_{1u} symmetry is thus (+2, +1, -1, -2, -1, +1), where numbers design charges at corners. The obtained charge distribution corresponds to an in-plane dipolar mode excited with an electric dipole moment along a line joining two opposite object apexes (see Fig. 2(a)). Since E_{1u} is a 2-dimensional irrep, a second charge eigenstate perpendicular to the first one exists. The latter is obtained by orthogonalization and corresponds to (0, +1, +1, 0, -1, -1). It is excited with an electric field normal to two opposite hexagon edges (see Fig. 2(b)). The orthogonalization procedure in conducted within the set of the projected basis vectors.

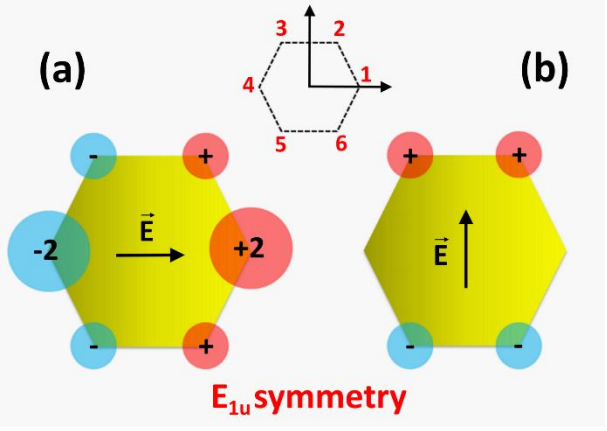

Figure 2 Symmetry adapted linear combinations (SALCs) corresponding to the two dipolar eigenmodes of a solid thin hexagon of D_{6h} symmetry.

As an experimental validation, PEEM images of the near optical field distribution of the E_{1u} plasmon mode in hexagonal Au MNPs are presented in Fig. 3. The objects under investigation are colloidal Au hexagons of in-plane height (altitude) of 150-200 nm and 16 ± 2 nm in thickness. Hexagon's thickness can be neglected in comparison to the in-plane dimensions. As a result, only the dipolar plasmon mode in the xy plane will be excited in the experimentally accessible near infrared wavelength range. The average distance between the particles is 1 ± 0.45 μm, so no significant object field coupling is expected. SEM image of the colloidal hexagons and their individual PEEM absorption spectra are given in ESM (Fig. S4 and Fig S7). The Au hexagons are excited with a laser beam at grazing incidence and at wavelength λ close to the dipolar resonance (λ = 850 nm). Fig. 3 details a comparison between PEEM results and group theory prediction. Experimental images are recorded at different exciting electric field orientations. Arrows in Fig. 3 represent the projection of the vectorial sum of the electric fields incident and reflected by the substrate under Fresnel conditions (see ESM). Additional PEEM images are given in ESM to valid the results reproducibility (Fig. S11). For an electric field normal to two opposite hexagon edges (Fig. 3(b), (d), (f), (h)), four corners exhibit clear photoemission signatures which corresponds to the dipolar eigenstate E_{1u}(0, +1, +1, 0, -1, -1) described in group theory. For an electric field whose direction is aligned on two opposite hexagon apexes (Fig. 3(a), (c), (e), (g), (i)), two hot spots are observed reminding the dipolar state E_{1u}(+2, +1, -1, -2, -1, +1). The four

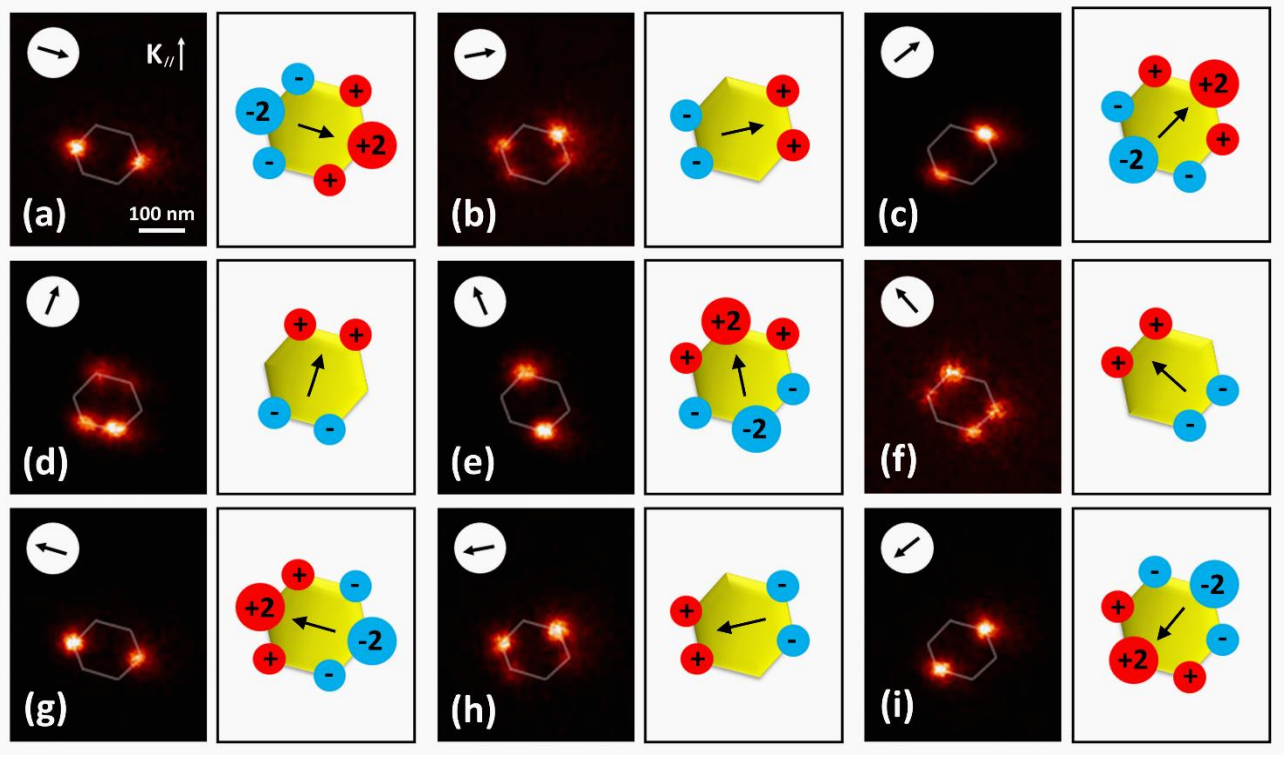

Figure 3 Polarization dependence of the dipolar plasmon mode of a 150 nm individual Au hexagon. Left column, PEEM imaging; right column, corresponding group theory predictions. Photon wavelength λ = 850 nm, beam incidence angle α = 72.5 ± 2°.

missing points are due to an insufficient dynamic range of the PEEM detection line. Indeed, being highly non-linear in nature [48] the photoemission signal exhibits a large dynamic range challenging the detector capabilities. Further considerations regarding the relative hot spot intensities and experimental details can be found in ESM (Fig. S14). So, for a 2D-MNP of hexagonal symmetry, a good agreement between PEEM near field maps and group theory is noted which further validates the analytical method in the case of objects of finite symmetry [49]. This method was also successfully applied to describe the plasmonic response of triangles (2D particles) [25] and cubes (3D particles) [26].

3.2. Particles of infinite symmetry

In the following, we extend and generalize the group theory approach to the case of particles of infinite symmetry. A particle of infinite symmetry exhibits an infinite number of symmetry elements making impossible the direct determination of the charge distribution by the previously detailed approach. Indeed, the problem is twofold. On one hand, at the surface of such an object there are no remarkable angular points where to attach s-atomic orbitals to mimic charges (no possible choice of the default basis). On the other hand, the projection operator corresponds to an intractable infinite sum of terms. As a general solution, we proposed to adopt a symmetry group that mimics an infinite group. In short, the particle surface is meshed so as to generate a high, but finite, number of symmetry elements; the object is thus transformed into an object of finite symmetry. For the choice of the default basis vector set, the s-atomic orbitals are attached at the different mesh points (vertices) and the projection operator turns into a finite sum allowing the previously detailed route toward the charge eigenstates calculations. As examples, the dipolar plasmon modes of nanodisks (2D particles) and nanospheres (3D particles) are presented, together with their experimental validations acquired by PEEM microscopy.

3.2.1. 2D particles: disks

As a first example, we consider a thin regular disk. A disk is invariant following a rotation of an arbitrary angle around its normal axis (z axis). It has also an infinite number of symmetry planes containing the principal rotation axis and an infinite number of C_2 rotation axis perpendiculars to the main rotation axis. The corresponding symmetry group is $D_{\infty h}$ (not considering any substrate). $D_{\infty h}$ is an infinite symmetry group, so it is impossible to determine directly the plasmon charge distribution using the group theory approach. Following the proposed strategy, the disk perimeter is meshed with line segments in order to reduce the disk into a polygon of finite symmetry and to generate angular points where to attach the initial basis set (set of s-atomic orbitals). In the present case, the disk is meshed using 32 points and the corresponding symmetry group is D_{32h} (see Fig. S2 in ESM). The choice of the number of mesh points is arbitrary; the precision of the result is proportional to the mesh step size (Fig.S15 in ESM). The plasmon charge distribution of the disk in-plane dipolar mode is determined by following the method employed in the case of hexagons. According to the character table of the D_{32h} point group [40], the external electric field transforms like the irrep E_{1u} and excites a dipolar mode of symmetry E_{1u} (see irrep products in ESM). The s-atomic orbitals are positioned at the 32 points obtained after meshing the disk perimeter. The application of the projection operator, corresponding to the irrep E_{1u}, to one of the equivalent s-atomic orbitals gives the charge eigenstate displayed in Fig. 4(a). According to the direction of the incident field, two areas of charge accumulation, opposite in sign and located at the periphery of the disc, can be defined. At each remarkable mesh point, the amount of

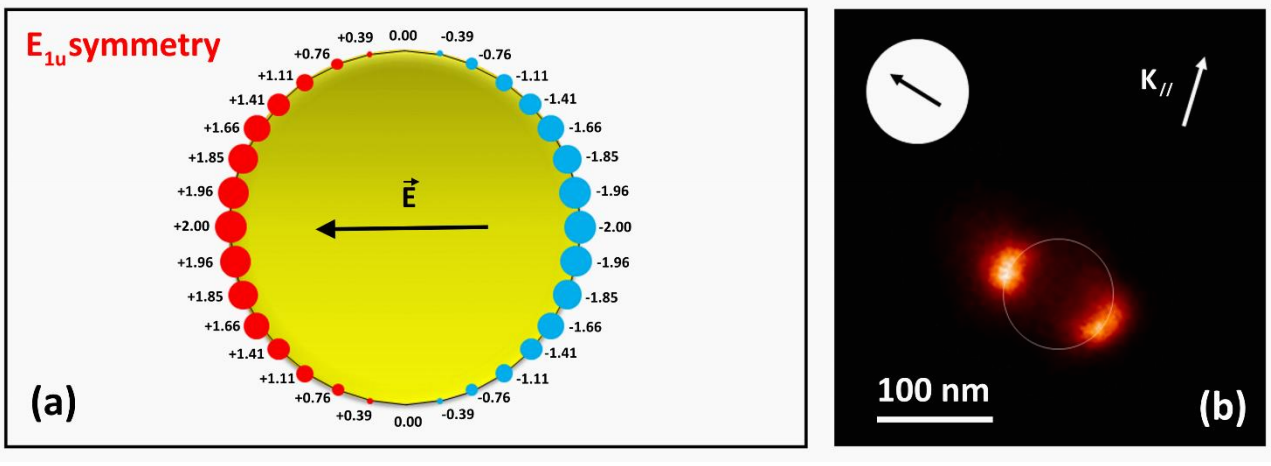

Figure 4 (a) Charge distribution of the in-plane dipolar plasmon mode of a disk obtained using group theory (32 points mesh grid). (b) PEEM map of the dipolar plasmon field distribution of a thin Au nanodisk of 92 nm in diameter. Photon wavelength λ = 780 nm, beam incidence angle α= 72.5±2°, 10°off *S* polarization.

charge decreases progressively from a maximum corresponding to the two points aligned on the incident electric field until cancelling in the direction perpendicular to the exciting field. This charge distribution corresponds to the cosine dependence inherited from the dipolar (l = 1, m= ± 1) spherical harmonics Yl^m involved in the description of the E_{1u} eigenstates[40].

The group theory result is compared to the ones obtained with PEEM microscopy (Fig. 4(b)). In more details, the plasmonic response of Au nanodisks of 92 ± 9 nm in diameter and 12 ± 3 nm in thickness is investigated using PEEM. The average distance between particles is 0.5 ± 0.2 μm preventing any significant plasmonic coupling between objects. SEM images and the absorption spectra of individual nanodisks are given in ESM (Fig. S5 and S8). The nanodisks are excited at grazing incidence α = 72.5 ± 2° with a laser beam at wavelength λ = 780 nm corresponding to the in-plane dipolar mode. The PEEM map shows that the plasmon field is distributed in two lobes along the nanodisk circumference, which is fully consistent with the group theory dipolar state E_{1u} and the previous studies [50, 51]. The experimental field distribution is more confined because of the non-linearity of the PEEM photoemission response (3-photons regime). Additional PEEM maps are available in ESM (Fig. S.12). In conclusion the experimental result validates the extended group theory method in the case of objects of infinite symmetry in 2D [49].

3.2.2. 3D particles: spheres

As a second example, we consider a basic regular 3D object, namely a sphere. In order to achieve a finite symmetry description, the particle surface is meshed like a Buckminsterfullerene molecule. Buckminsterfullerene, called also fullerene C_{60}, is a spherical molecule composed of 20 hexagons and 12 pentagons with a carbon atom at each vertex of each polygon and a bond along each polygon edge. All vertices are equivalent by symmetry [52]. In short, a buckminsterfullerene has a structure that resembles a soccer ball. After meshing, a spherical particle exhibits a structural symmetry corresponding to the I_h point group (see Fig. S3 in ESM). According to the corresponding character table [40], the irrep describing the symmetry of the exciting electric field $\overrightarrow{E_{ext}}$ = ($E_{ext,x}$, $E_{ext,y}$, $E_{ext,z}$) is T_{1u}. T_{1u} corresponds to a mode with a non-zero electric dipole moment and can be excited by the external electric field $\overrightarrow{E_{ext}}$ (bright mode). The irrep products are given in ESM. For the initial choice of the basis vector set, s-atomic orbitals are placed at the vertex positions, i.e. the corresponding carbon atom positions of the C_{60} molecules. The plasmon charge averaged on each hexagon and pentagon surface areas, obtained by projection of one of the s-atomic orbitals on the irrep T_{1u}, is presented in Fig. 5(a). At dipolar plasmon resonance, the plasmonic charges (SALC eigenstate) are distributed over two hemispheres of opposite signs aligned on the incident electric field direction. This theoretical result is in line with those (*i*) of the analytic description of a sphere in the quasi-static regime [53,54] and (*ii*) of the more sophisticated and demanding electromagnetic simulations conducted by FDTD [55, 56], DDA [57] and BEM [49].

An experimental validation is carried out by mapping the optical near field in a Au colloidal nanospheres using PEEM. Au nanospheres of 98 ± 1.6 nm in diameter are excited in the visible at a wavelength λ = 540 nm close to the dipolar resonance under grazing incidence α = 72.5 ± 2° and in *S* polarization. For the considered illumination geometry, excitation in *S* polarization corresponds to the excitation of the sphere equatorial plane, where the surface charge separation can be more easily spotted experimentally. Indeed, a *P* polarization would correspond to a polar plane excitation for which the charge separation will be difficult to ascertain since the electron signal is collected along the polar axis (normal substrate axis). The average distance between close sphere neighbours is about 0.6 ± 0.1 μm, so one expects no significant plasmonic coupling between the particles. SEM images of the nanospheres together with individual absorption spectra are given in Fig. S6 and S9 in the ESM. The field distribution acquired with PEEM microscopy is represented in Fig. 5(b). The PEEM map shows a confinement of the plasmon field according to two lobes around the sphere, aligned along the direction of the exciting electric field. These experimental results are in agreement with those obtained using group theory which validates the theoretical method in the case of 3D objects of infinite symmetry [49]. Additional PEEM images are given in ESM (Fig. S13).

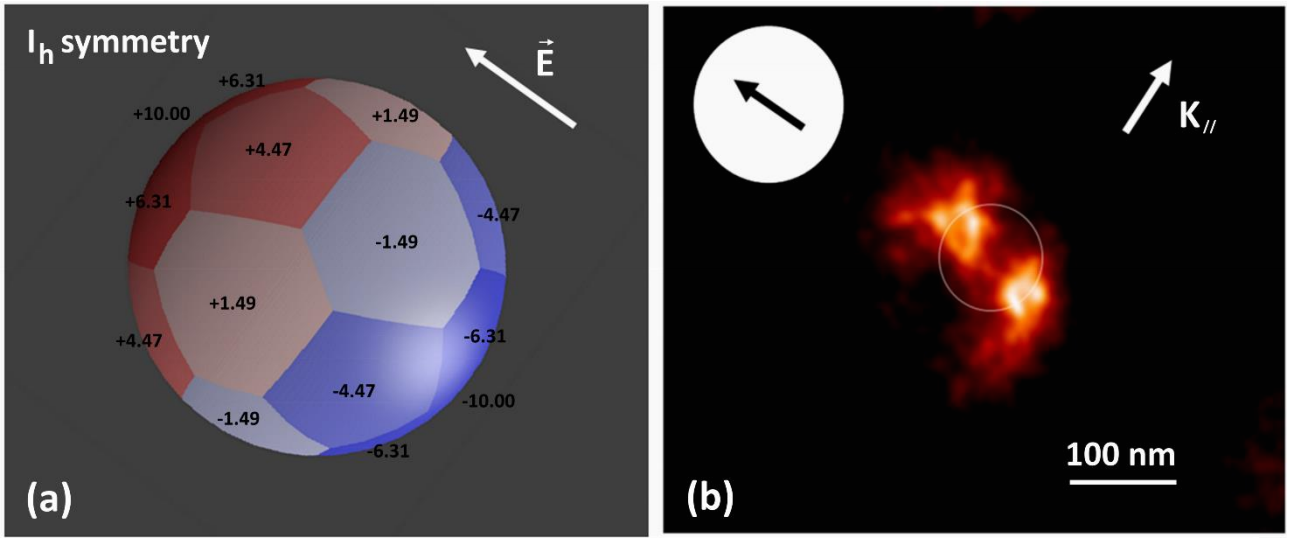

Figure 5 (a) Charge distribution of the dipolar plasmon mode in a sphere obtained using group theory (mesh grid in the form of a fullerene C_{60} molecule, negative charge in blue, positive in red. (b) PEEM map of the dipolar plasmon field distribution of a Au nanosphere of 98 nm in diameter. Photon wavelength λ = 540 nm, beam incidence angle α = 72.5 ± 2°, *S* polarization.

4. Conclusions

Group theory offers the possibility to predict and to investigate the plasmonic responses of MNPs by a hand calculation. In this article, we have demonstrated, through several examples, that group theory can be successfully applied to predict the plasmonic hot spots distribution in particle of finite (hexagon) and infinite (disk, sphere) symmetry point groups. The symmetry approach is confirmed by high-resolution subwavelength near field mapping conducted by PEEM microscopy. This investigation confirms the general character of the group theory method previously applied to finite symmetry MNPs [25, 26].

Further extensions of the group theory approach can be envisaged. First, the present examples correspond to the determination of plasmon eigenstates of dipolar character of objects of simple canonical shapes. In this case the choice of an initial orbital basis is simple, but difficulties arise when one considers higher order plasmonic modes of the particle. One way to circumvent this difficulty consists in the meshing of the objects using fullerene molecules. Indeed, depending on the number of carbon atoms, a fullerene molecule can adopt a geometrical shape of various symmetries: a sphere, an ellipsoid, a rod, etc [52]. These molecules possess a finite number of symmetry elements. So, access to higher order resonance modes is made possible. Second, the present work deals with objects of various symmetry point groups and a simple linearly polarized excitation light wave. Another perspective is the use of the group theory approach to predict the plasmonic behaviour of one simple shape MNP excited with an electromagnetic wave of complex symmetry: elliptically polarized [49] or presenting an orbital angular momentum for instance.

Conflicts of interest

There are no conflicts to declare.

Acknowledgements

Part of the developments regarding the infinite point group symmetry comes out from a fruitful exchange with Paul Walton and Alessandro Paradisi from the University of York, UK. The CEA authors thank them sincerely for their solid contribution. The CEA authors acknowledge financial support by the French National Agency (ANR) in the frame of its program in Nanosciences and Nanotechnologies (PEEM Plasmon Project ANR-08-NANO-034, ANR P2N 2013-Samiré), Nanosciences Île-de-France (PEEM Plasmonics project), the "Triangle de la Physique" (PEPS Project 2012-035T) and the doctoral school "Ecole Doctorale Ondes et Matière (EDOM)".

Electronic Supplementary Material (ESM): Supplementary material (Symmetry elements, further details of the group theory calculation, SEM imaging, PEEM absorption spectra, calculation of the true exciting field in PEEM, additional PEEM images) is available in the online version of this article at http://dx.doi.org/10.1007/s12274

References

[1] Garcia, M. A. Surface plasmons in metallic nanoparticles: fundamentals and applications. *J. Phys. D: Appl. Phys*. **2011**, 44, 283001.

[2] Kong, X.-T.; Wang, Z.; Govorov, A. O. Plasmonic nanostars with hot spots for efficient generation of hot Electrons under solar illumination. *Adv. Opt. Mater*. **2017**, 5, 1600594.

[3] Wei, H.; Xu, H. Hot spots in different metal nanostructures for plasmon-enhanced Raman spectroscopy. *Nanoscale*. **2013**,5, 10794-10805.

[4] Yanik, A. A.; Cetin, A. E.; Huang, M.; Artar, A.; Mousavi, S. H.; Khanikaev, A.; Connor, J. H.; Shvets, G.; Altug, H. Seeing protein mono- layers with naked eye through plasmonic Fano resonances. *Proceedings of the National Academy of Sciences*. **2011**, 108, 11784-11789.

[5] Wang, H. Plasmonic refractive index sensing using strongly coupled metal nanoantennas: Nonlocal limitations. *Sci. Rep*. **2018**, 8, 9589.
[6] Willets, K.; Van Duyne, R. Localized surface plasmon resonance spectroscopy and sensing. *Annu. Rev. Phys. Chem*. **2007**, 58, 267-297.
[7] Baffou, G.; Quidant, R. Thermo-plasmonics: using metallic nanostructures as nano-sources of heat. *Laser Photonics Rev*. **2013**, 7, 171-187.
[8] Palermo, G.; Cataldi, U.; Condello, A.; Caputo, R.; Bürgi, T.; Umeton, C.; De Luca, A. Flexible thermo-plasmonics: an opto-mechanical control of the heat generated at the nanoscale. *Nanoscale*. **2018**, 10, 16556-16561.
[9] Shi, X.; Ueno, K.; Takabayashi, N.; Misawa, H. Plasmon-enhanced photocurrent generation and water oxidation with a gold nanoisland-loaded titanium dioxide photoelectrode. *J. Phys. Chem. C*. **2013**, 117, 2494-2499.
[10] Oshikiri, T.; Ueno, K.; Misawa, H. Plasmon-induced ammonia synthesis through nitrogen photofixation with visible light irradiation. *Angew. Chem., Int. Ed*. **2014**, 53, 9802-9805.
[11] Labouret, T.; Audibert, J.-F.; Pansu, R. B.; Palpant, B. Plasmon-assisted production of reactive oxygen species by single gold nanorods. *Small*. **2015**, 11, 4475-4479.
[12] Vankayala, R.; Huang, Y.-K.; Kalluru, P.; Chiang, C.-S.; Hwang, K. C. First demonstration of gold nanorods-mediated photodynamic therapeutic destruction of tumors via near infra-red light activation. *Small*. **2014**, 10, 1612-1622.
[13] Zhao, T.; Shen, X.; Li, L.; Guan, Z.; Gao, N.; Yuan, P.; Yao, S. Q.; Xu, Q.-H.; Xu, G. Q. Gold nanorods as dual photo-sensitizing and imaging agents for two-photon photodynamic therapy. *Nanoscale*.**2012**, 4, 7712-7719.
[14] Wang, S.; Xi, W.; Fuhong, C.; Zhao, X.; Xu, Z.; Qian, J.; He, S. Three-photon luminescence of gold nanorods and its applications for high contrast tissue and deep in vivo brain imaging. *Theranostics*. **2015**, 5, 251-266.
[15] Cheng, Y.-H.; Tam, T. S.-C.; Chau, S.-L.; Lai, S. K.-M.; Tang, H.-W.; Lok, C.-N.; Lam, C.-W.; Ng, K.-M. Plasmonic gold nanoparticles as multifaceted probe for tissue imaging. *Chem. Commun*. **2019**, 55, 2761-2764.
[16] Ozbay, E. Plasmonics: Merging photonics and electronics at nanoscale dimensions. *Science*. **2006**, 311, 189-193.
[17] Talove, A.; Hagness, S. *Computational electrodynamics: The finite-difference time-domain method*; Artech House, 2005.
[18] Yee, K. S. Numerical Solution of Initial Boundary Value Problem Involving Maxwell's Equations in Isotropic Media. *IEEE Trans. Antennas and Propagation*. **1966**, AP-14, 302-307.
[19] Montgomery, J. M.; Lee, T.-W.; Gray, S. K. Theory and modeling of light interactions with metallic nanostructures. *J. Phys.: Condens. Matter*. **2008**, 20, 323201.
[20] Yurkin, M.; Hoekstra, A. The discrete dipole approximation: An overview and recent developments. *J. Quant. Spectrosc. Radiat. Transfer*. **2007**, 106, 558-589.
[21] Draine, B. T.; Flatau, P. J. Discrete-Dipole Approximation For Scattering Calculations. *J. Opt. Soc. Am. A*. **1994**, 11, 1491-1499.
[22] Cotton, *F. Chemical Applications of Group Theory*, *3rd Edition*; John Wiley & Sons, Incorporated, 2015.
[23] Volatron, F.; Chaquin, P. *La théorie des groupes en chimie; LMD Chimie*; De Boeck Supérieur, 2017.
[24] Walton, P. *Beginning Group Theory for Chemistry*; OUP Oxford, 1998.
[25] Awada, C.; Popescu, T.; Douillard, L.; Charra, F.; Perron, A.; Yockell-Lelièvre, H.; Baudrion, A.-L.; Adam, P.-M.; Bachelot, R. Selective Excitation of Plasmon Resonances of Single Au Triangles by Polarization- Dependent Light Excitation. *J. Phys. Chem. C*. **2012**, 116, 14591-14598.
[26] Mitiche, S.; Marguet, S.; Charra, F.; Douillard, L. Near-Field Localization of Single Au Cubes: A Group Theory Description. *J. Phys. Chem. C*. **2017**, 121, 4517-4523.
[27] Xiong, G.; Shao, R.; Peppernick, S. J.; Joly, A. G.; Beck, K. M.; Hess,W. P.;Cai, M.; Duchene, J.; Wang, J. Y.; Wei, W. D. Materials applications of photoelectron emission microscopy. *JOM*. **2010**, 62, 90-93.
[28] Haight, R.; Ross, F.; Hannon, J. *Handbook of Instrumentation and Techniques for Semiconductor Nanostructure Characterization*; World Scientific, 2012.
[29] Rodríguez-Fernández, J.; Pérez-Juste, J.; Mulvaney, P.; Liz-Marzán, L. M. Spatially-Directed Oxidation of Gold Nanoparticles by Au(III) CTAB Complexes. *J. Phys. Chem. B.* **2005**, 109, 14257-14261.
[30] Ruan, Q.; Shao, L.; Shu, Y.; Wang, J.; Wu, H. Growth of Monodisperse Gold Nanospheres with Diameters from 20 nm to 220 nm and Their Core/Satellite Nanostructures. *Adv. Opt. Mater*. **2014**, 2, 65-73.
[31] Young, K. L.; Jones, M. R.; Zhang, J.; Macfarlane, R. J.; Esquivel-Sirvent, R.; Nap, R. J.; Wu, J.; Schatz, G. C.; Lee, B.; Mirkin, C. A. Assembly of reconfigurable one-dimensional colloidal superlattices due to a synergy of fundamental nanoscale forces. *Proc. Natl. Acad. Sci*. **2012**, 109, 2240-2245.
[32] *Surface cleaning and modification by UV light* [Online]. https://www.crystec.com/sentechf.htm (Accessed May 01, 2019).
[33] Douillard, L.; Charra, F.; Fiorini, C.; Adam, P.-M.; Bachelot, R.; Kostcheev, S.; Lerondel, G.; Lamy De La Chapelle, M.; Royer, P. Optical properties of metal nanoparticles as probed by photoemission electron microscopy. *J. Appl. Phys.* **2007**, 101, 083518-083518.
[34] Douillard, L.; Charra, F. High-resolution mapping of plasmonic modes: Photoemission and scanning tunnelling luminescence microscopies. *J. Phys. D: Appl. Phys*. **2011**, 44, 464002.
[35] Douillard, L.; Charra, F. Photoemission electron microscopy, a tool for plasmonics. *J. Electron Spectrosc. Relat. Phenom*. **2013**, 189, 2429.
[36] Schmidt, O.; Bauer, M.; Wiemann, C.; Porath, R.; Scharte, M.; Andreyev, O.; Schönhense, G.; Aeschlimann, M. Time-resolved two photon photoemission electron microscopy. *Appl. Phys. B.***2002**, 74, 223-227.
[37] Losquin, A.; T. A. Lummen, T. Electron microscopy methods for space-, energy-, and time-resolved plasmonics. *Frontiers of Physics.* **2017**, 12, 127301.
[38] Kubo, A.; Onda, K.; Petek, H.; Sun, Z.; Jung, Y. S.; Kim, H. K. Femtosecond Imaging of Surface Plasmon Dynamics in a Nanostructured Silver Film. *Nano Lett*. **2005**, 5, 1123-1127.
[39] Bauer, E. *Surface Microscopy with Low Energy Electrons*; Springer New York, 2014.
[40] *Character Tables for Point Groups used in Chemistry* [Online], http://gernot-katzers-spice-pages.com/character_tables/index.html (Accessed May 01, 2019).
[41] Zhang, W.; Gallinet, B.; Martin, O. J. F. Symmetry and selection rules for localized surface plasmon resonances in nanostructures. *Phys. Rev. B.***2010**, 81, 233407.
[42] Kociak, M.; Stéphan, O.; Gloter, A.; Zagonel, L. F.; Tizei, L. H.; Tencé, M.;March, K.; Blazit, J. D.; Mahfoud, Z.; Losquin, A.; Meuret, S.; Colliex, C. Seeing and measuring in colours: Electron microscopy and spectroscopies applied to nano-optics. *C. R. Phys.***2014**, 15, 158-175.
[43] Nelayah, J.; Gu, L.; Sigle, W.; T Koch, C.; Pastoriza-Santos, I.; Liz-Marzan, L.; A van Aken, P. Direct imaging of surface plasmon resonances on single triangular silver nanoprisms at optical wavelength using low-loss EFTEM imaging. *Opt. Lett*. **2009**, 34, 1003-1005.
[44] Yang, J.; Sun, Q.;Yu, H.; Ueno, K.; Misawa, H.; Gong, Q. Spatial evolution of the near field distribution on planar gold nanoparticles with the excitation wavelength a cross dipole and quadrupole modes. *Photonics Res.* **2017**, 5, 187.
[45] Gómez-Medina, R.; Yamamoto, N.; Nakano, M.; de Abajo, F. J. G. Mapping plasmons in nanoantennas via cathodoluminescence. *New J. Phys* .**2008**, 10, 105009.
[46] Nicoletti, O.; de la Peña, F.; K Leary, R.; Holland, D.; Ducati, C.; A Midgley, P. Three-dimensional imaging of localized surface plasmon resonances of metal nanoparticles. *Nature*. **2013**, 502, 80-84.
[47] Kim, D.-S.; Heo, J.; Ahn, S.-H.; Han, S. W.; Yun, W. S.; Kim, Z. H. Real-Space Mapping of the Strongly Coupled Plasmons of Nanoparticle Dimers. *Nano Lett*. **2009**, 9, 3619-3625.

[48] Awada, C.; Barbillon, G.; Charra, F.; Douillard, L.; Greffet, J.-J. Experimental study of hot spots in gold/glass nanocomposite films by photoemission electron microscopy. *Phys. Rev. B*. **2012**, 85, 045438.
[49] Mitiche, S. Plasmonique, un outil pour l'ingénierie du champ électromagnétique aux petites échelles: Manipulation du champ proche optique. Ph.D. thesis, Université Paris-Saclay, Gif-sur-Yvette, France, 2018.
[50] Aeschlimann, M.; Brixner, T.; Fischer, A.; Hensen, M.; Huber, B.; Kilbane, D.; Kramer, C.; Pfeiffer, W.; Piecuch, M.; Thielen, P. Determination of local optical response functions of nanostructures with increasing complexity by using single and coupled Lorentzian oscillator models. *Appl. Phys. B.* **2016**, 122, 1-11.
[51] Yang, J.; Sun, Q.; Yu, H.; Ueno, K.; Misawa, H.; Gong, Q. Spatial evolution of the near-field distribution on planar gold nanoparticles with the excitation wavelength across dipole and quadrupole modes. *Photon. Res.* **2017**, 5, 187-193.
[52] Schwerdtfeger, P.; Wirz, L. N.; Avery, J. The topology of fullerenes. *Wiley Interdiscip. Rev.: Comput. Mol. Sci.* **2015**, 5, 96-145.
[53] Maier, S. *Plasmonics: Fundamentals and Applications*; Springer US, 2007.
[54] Novotny, L.; Hecht, B. *Principles of Nano-Optics*; Cambridge University Press, 2006.
[55] Katyal, J.; Soni, R. Field Enhancement Around Al Nanostructures in the DUV-Visible Region. *Plasmonics.* **2015**, 10, 1729-1740.
[56] Shautsova, V. I.; Zhuravkov, V. A.; Korolik, O. V.; Novikau, A. G.; Shevchenko, G. P.; Gaiduk, P. I. Effect of Interparticle Field Enhancement in Self-Assembled Silver Aggregates on Surface-Enhanced Raman Scattering. *Plasmonics*. **2014**, 9, 993-999.
[57] Schatz, G. C. Using theory and computation to model nanoscale properties. *Proc. Natl. Acad. Sci*. **2007**, 104, 6885-6892.